Int. J. Electrochem. Sci., 16 **(2021)** Article ID: 210212, doi: 10.20964/2021.02.34

International Journal of
ELECTROCHEMICAL
SCIENCE
www.electrochemsci.org

Zinc Stannate as anode and Pyrrolidinium-Based Room Temperature Ionic Liquid as electrolyte for Lithium-ion Cells

Diego Quezada[1,*], *Jessica Honores*[2], *Domingo Ruiz-León*[3]

[1] Facultad de Ingeniería, Institute of Applied Chemical Sciences, Universidad Autónoma de Chile, El Llano Subercaseaux 2801, 5° piso, San Miguel, Santiago, Chile.
[2] Facultad de Química y de Farmacia, Pontificia Universidad Católica de Chile, Av. Vicuña Mackenna 4860, Macul, Santiago, Chile
[3] Departamento de Química de los Materiales, Facultad de Química y Biología, Universidad de Santiago de Chile, Av. Libertador Bernardo O´Higgins 3363, Santiago, Chile.
[*]E-mail: diego.quezada@uautonoma.cl

Received: 2 July 2020 / *Accepted:* 10 September 2020 / *Published:* 31 December 2020

With the aim to design safer batteries, pyrrolidinium-based room temperature ionic liquids (RTIL) have been used as electrolytes in Li-ion batteries using zinc stannate as the anodic material. The lithium diffusion coefficients were calculated using Electrochemical Impedance Spectroscopy (EIS) data and were 2.37 x 10^{-12} cm^2s^{-1} for MPPyrTFSI and 1.29 x 10^{-12} cm^2s^{-1} for BMPyrTFSI. The performance of the device strongly depended on the cation chemical structure, yielding different specific capacity values of 306.3 $mAhg^{-1}$ for BMPyrTFSI and 269.2 $mAhg^{-1}$ for MPPyrTFSI.

Keywords: Lithium-ion cells, Ionic Liquids, Zinc Stannate

1. INTRODUCTION

The creation of rechargeable lithium-based batteries has dramatically changed the concept of portable electronics and is now a starting point for further development of the power supply of small electronics. The presence of Li-ion batteries in consumable electronics is so widespread that it has almost completely replaced alkaline, Ni-Cd and Ni-MH batteries in many daily used electronic devices [1,2].

Since the first Li-ion battery was released in 1991 by SONY [3,4], the development of the technology has allowed for an increase in energy density at an estimated rate of 5 $Whkg^{-1}$ every year, currently reaching approximately 160 $Whkg^{-1}$ more than twice the energy density of the initial 18650 devices. Even though this value allows an efficient performance in small electronics and low-power applications, it is not enough to meet the needs of total vehicle electrification (500-700 $Whkg^{-1}$) [5], and this issue remains a challenge that scientific community must solve in the coming years [3,6,7]. It is

crucial to understand that advances in LIB technology will only be possible if an integrated effort is achieved, this is, advances in the performance of every component of the LIB, including the anode, cathode and electrolyte. In this sense, the creation of new materials as innovative electrodes and electrolytes [8], as well as the development of new architectures for positive [9,10] and negative [11] electrode materials with a high capacity and operating at a high current, can be considered a valuable step in the right direction.

In this context, investigations into cathode materials are probably the effort that has made the most promising advances considering that 25 years ago $LiCoO_2$ was the standard cathode material, even though [12] it presents a high cost and low abundance, which together with its toxicity and safety issues, render this cathode impossible for use in larger devices that could give energy to vehicles and stationary storage devices. The current standard can be represented by a large family of nanostructured layered oxides, in particular, lithium-rich phases of layered multimetallic oxides [13–15]. A good example is NMC ($Li[NiMnCo]O_2$), which can operate at a high potential (exceeding 4.8 V) with a theoretical capacity of 240 $mAhg^{-1}$ [16]. The anodic materials can be analysed in a similar way; however, the first LIB carbon electrodes have shown low toxicity, high abundance, low cost and a capacity of approximately 370 $mAhg^{-1}$. Due to their interesting properties, stannates have recently been evaluated as anodic materials in LIBs [17]. In particular, zinc stannates have been recognized for having interesting features, including its affordable price and its high neat charge capacity (approximately 1200 $mAhg^{-1}$) [18,19]. The latter is favoured by the formation of multiple intermediate redox states that can allow the intercalation of up to 12 lithium atoms on its crystalline structure, resulting in a massive volume change in the solid that, over the long term, results in irreversible chemical changes to the electrode [20].

Considering the last statement, the main restriction to increasing the energy density of lithium-ion batteries is the need to fulfil the criteria of safety and credibility; in other words, for LIBs to be successfully exploited in the large-scale market of electric/hybrid electric transportation, the power sources must be non-flammable upon long-term cycling, as well as robust enough to resist severe stressing operation at high/low temperatures and in fast charge/discharge current regimes [21]. All of these characteristics are mainly determined by the nature of the electrolyte, whose development has been limited in most cases to the application of lithium salts dissolved in organic carbonates and their derivates, with the latter component being flammable and potentially dangerous at high temperatures. Alternatives to organic electrolytes have been explored from polymer electrolytes to gel-type electrolytes and ending in completely solid-state batteries, in which the electrolyte presents a solid interface for ionic conduction [22,23]. In general terms, an ideal electrolyte must be non-flammable with a sufficiently high Li+ ion mobility; a low reactivity towards Li, Cu and Al (common metallic LIB components) [24,25]; and a wide electrochemical stability window, which could ensure electrochemical stability over a broad range of electrochemical potentials [26,27]. An interesting candidate to fulfil these requirements is ionic liquids, which are room temperature molten salts often composed of an organic cation and an inorganic anion, and due to their ionic nature, this solvent class presents a negligible vapour pressure and non-flammablity. Depending on their composition, ionic liquids can provide an electrochemical window of up to 6 V (for certain combinations of cations and anions), considerably wider than that of organic carbonates [24,28]. However, the main problem with common ionic liquids is the ionic conductivity, which is smaller than that of common electrolytic solutions [24,29].

It is well known that the nominal capacity of an electrochemical energy storage device is mainly determined by the active materials that are forming both the anode and cathode. Thus, the development of high-capacity materials is a crucial point to develop devices with a higher nominal capacity. In this work, the performance of high-capacity ceramic materials such as Zn stannates is tested as the anodic material with pyrrolidinium-based ionic liquids as the electrolyte to obtain higher capacities in a safer and organic-solvent-free lithium battery.

2. EXPERIMENTAL

2.1. Materials

Zinc stannate (Zn_2SnO_4), or ZTO, was synthesized and characterized following a previously reported method [30]. Briefly, tin tetrachloride ($SnCl_4*5H_2O$) and zinc chloride ($ZnCl_2$) were dissolved in double distilled water forming two transparent solutions, and after complete dissolution, tin tetrachloride was added dropwise to the zinc tetrachloride solution. As a mineralizer, a sodium carbonate ($NaCO_3$) solution was added dropwise to the previous mixture under continuous magnetic stirring. The formed slurry was transferred to a Teflon-lined stainless-steel autoclave and subjected to hydrothermal conditions at 200°C for 30 hours. After the reaction, the reactor was cooled at room temperature, and the resulting precipitate was rinsed with double distilled water and ethanol. The solid product was dried overnight at 60°C and then characterized by XRD.

2.2. Electrochemical Measurements

The electrodes were prepared using a dispersion of N-methyl-2-pyrrolidone (NMP, solvent) the as-prepared Zn_2SnO_4 (80 wt%), carbon black (20 wt%), and polyvinylidene fluoride (PVDF, binder). The obtained slurry was uniformly dispersed on a Cu foil forming a thin film and dried under vacuum at 65°C for 12 hours. The electrode was then pressed for 3 hours by applying 2 tons/cm^2 of pressure and then cut into discs (d: 10 mm). The average mass loading of each electrode was 1.46 mg/cm^2 (1.17 mg/cm^2 of active material). Coated Cu electrodes were used as the anode in CR2032 coin cells. Cells were assembled in an Ar-filled glove box maintaining oxygen and water content lower than 1 ppm. Li half-cells were assembled with Li metal as the counter and reference electrodes, a 1 M LiNTF2 solution in 1-methyl-1-propylpyrrolidinium bis(trifluoromethanesulfonyl)imide ([Mppyr][TFSI]) or 1-butyl-1-propylpyrrolidinium bis(trifluoromethanesulfonyl)imide ([Bmpyr][TFSI]) was used as the electrolyte, and a Celgard 2400 membrane was employed as the separator. For comparison purposes butylmethylimidazolium and ethylmethylimidazolium bis(trifluoromethanesulfonyl)imide ([Bmim][TFSI] and [Emim][TFSI]) was also used. Galvanostatic charge-discharge tests were performed on a Neware BTS4000 battery testing instrument with a voltage range of 0.05–3 V versus Li/Li$^+$ at room temperature. Cyclic voltammetry (CV) tests were measured on a Gamry Reference Module 600C electrochemical workstation (Gamry) at a scan rate of 0.1 mV/s. Electrochemical impedance

spectroscopy (EIS) was performed on the cells over a frequency range from 100 kHz to 0.01 Hz using a Gamry Reference Module 600C electrochemical workstation with an AC signal amplitude of 10 mV.

3. RESULTS AND DISCUSSION

3.1. XRD Characterization

The purity and homogeneity of Zn_2SnO_4 was evaluated by XRD. A comparison of the XRD powder pattern (Figure 1) with the database reference confirms the purity and the homogeneity of the sample. Additionally, the obtained XRD powder pattern was compared and analysed using the Rietveld method. The analysis of the structure shows that the synthesized phase corresponds to an inverse spinel, which crystallized in a cubic system with the space group *F d 3 m*. The atomic arrangement for this type of spinel is $Zn_{tet}(Zn, Sn)_{oct}O_4$, and these calculations fully agree with our previously reported work [30].

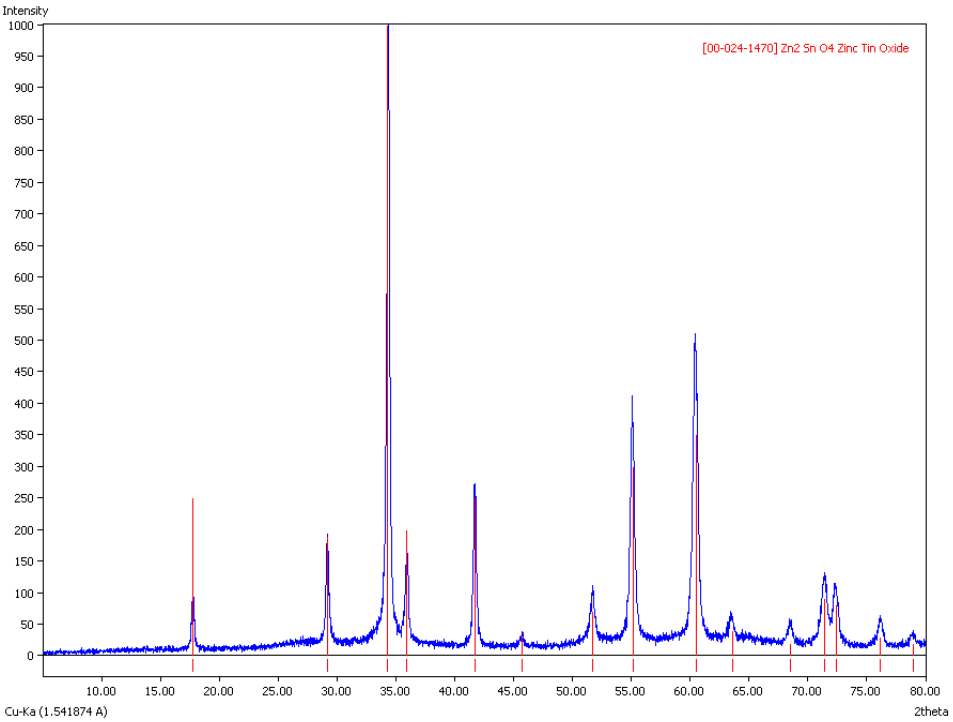

Figure 1. XRD pattern of Zn_2SnO_4 compared with the database pattern.

3.2 EIS results

Imidazolium ionic liquids are without a doubt the most studied alternative to replace common electrolytes in lithium-ion batteries [24,31]; however, their high viscosity and low conductivity make this kind of electrolyte a less practical alternative than other ionic liquids designed to minimize the previously mentioned issues. A good example of this new generation of molten salts is pyrrolidinium-based ionic liquids, whose properties have been well described elsewhere [32–34]. As a comparative study, the electrochemical properties of commonly used imidazolium-based ionic liquids such as 1-butyl-3-methylimidazolium bis(trifluoromethylsulfonyl)imide ([BMIm][TFSI]) and 1-ethyl-3-

methylimidazolium bis(trifluoromethylsulfonyl)imide ([EMIm][TFSI]) were measured and compared to the properties of the pyrrolidinium-based ionic liquids used in this work.

Electrochemical impedance spectroscopy experiments were carried out between 10^{-2} and 10^{5} Hz. Nyquist plots of cells based on [Bmpyr][TFSI] and [Mppyr][TFSI], as well as two imidazolium ionic liquids included as a comparison, are shown in figure 2.

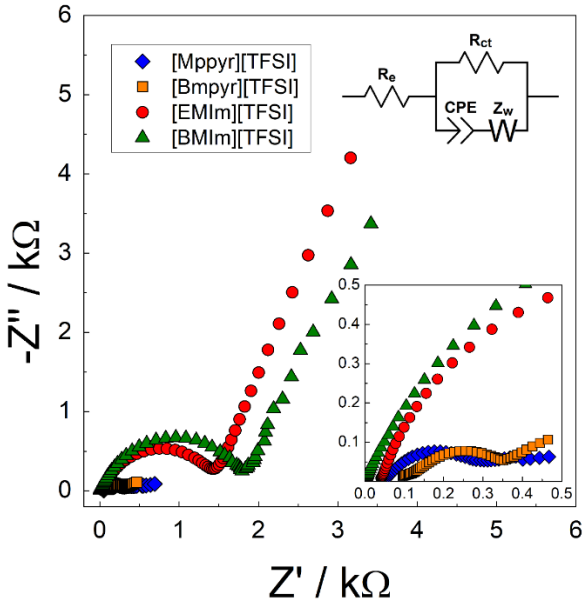

Figure 2. Nyquist plots of the batteries studied EIS was carried out over a frequency range from 100 kHz to 0.01 Hz with an AC signal amplitude of 10 mV. Insert: Equivalent circuit modelled for all the prototypes.

As seen in figure 2, Nyquist plots of all the cells studied present an imperfect semicircle in the high-frequency region and a straight line in the low-frequency region, and hence, it can be inferred that all of the devices studied can be represented by the same equivalent circuit.

Table 1. Summary of the relevant information obtained from the EIS experiments.

Element	[Bmpyr][TFSI]	[Mppyr][TFSI]	[BMIm][TFSI]	[EMIm][TFSI]
R_e / **Ω**	92.06	47.92	3.89	41.12
R_p / **Ω**	335.2	319.4	1609.2	1135.6
γ_0 / Ss^a	83.25 x 10^{-6}	53.45 x 10^{-6}	2.75 x 10^{-6}	2.33 x 10^{-6}
α	0.51	0.63	0.78	0.84
W_d / $Ss^{1/2}$	2.369 x 10^{-3}	3.20 x 10^{-3}	4.34 x 10^{-4}	3.65 x 10^{-4}

In general, the Z_{re} axis value of the high-frequency point can be associated with the electrolyte resistance (R_e), and the numerical value of the semicircle diameter on the Z_{re} axis can be interpreted as

the charge transfer resistance (R_p). Considering these facts, a fast analysis of figure 2 indicates that imidazolium ionic liquids perform worse as an electrolyte than do the pyrrolidinium-based ionic liquids.

By modelling the EIS results with the equivalent circuit shown in the inset of figure 2, a more precise approximation to the values of each element can be made. The magnitude associated with each element was fitted and adjusted to the lowest error percentage possible, usually less than 5%. The obtained values are summarized in Table 1.

The resistance of each electrolyte to the charge transfer process is represented by the R_p element in the equivalent circuit depicted in the inset of figure 2. The value obtained for R_p for each of the ionic liquids tested offers a suitable basis for comparison in terms of the capacity of each electrolyte to offer an efficient charge transfer and therefore an easier redox reaction at the working electrode. In this context, imidazolium ionic liquids present higher values, while [BMIm][TFSI] is the most resistive, followed by [EMIm][TFSI], whose values remain the same order of magnitude. On the other hand, pyrrolidinium ionic liquids present a considerably lower resistance to charge transfer but provide a higher intrinsic resistance (R_e). This fact implies that the pyrrolidinium ionic liquids used in this work are a worse electronic conductor but a better ionic conductor and are therefore a more suitable media for lithiation and delithiation processes. Previous works have explained that pyrrolidinium ionic liquids allow lithium to be cycled with a high degree of reversibility, and this phenomenon is achieved due to a stable and uniform SEI, which allows for the selective diffusion of Li^+ ions [35,36].

The diffusion process in the ionic liquids was studied using the Warburg impedance values obtained from the EIS experiments. The diffusion coefficient of Li^+ was then calculated using the relation shown in Eqn. 1.

$$D = \frac{R^2T^2}{2A^2n^4F^4C^2\sigma^2} \qquad (1)$$

where R is the gas constant, T is the absolute temperature, n is the number of electrons per molecule oxidized, A is the geometrical area of the electrode, F is the Faraday constant, C is the concentration of the diffusive species, and σ is the Warburg impedance factor, which is obtained using Eqn. 2.

$$\sigma = \frac{1}{\sqrt{2}\gamma_0} \qquad (2)$$

where the Warburg admittance value (γ_0) is obtained from the fitting process previously mentioned.

The diffusion coefficient of Li^+ in the ionic liquids studied was calculated using Eqn. 1 and the values of γ_0 shown in Table 1; the obtained values are summarized in Table 2.

Table 2. Calculated lithium diffusion coefficients.

	Diffusion coefficient, D_{Li} / cm^2s^{-1}
[Bmpyr][TFSI]	1,29 x 10^{-12}
[Mppyr][TFSI]	2,37 x 10^{-12}
[BMIm][TFSI]	4,34 x 10^{-14}
[EMIm][TFSI]	3,08 x 10^{-14}

According to Table 2, the diffusion coefficients obtained from the studied ionic liquids are strongly dependent on the main structure of the electrolyte cation, being approximately two orders of magnitude smaller in the case of the imidazolium ionic liquids. Regarding the values obtained for the pyrrolidinium ionic liquids, they are considerably smaller than the values reported in the literature [2,22,24,31,34,37–41], which are commonly approximately 10^{-10} cm^2s^{-1} when conventional electrodes and molecular electrolytes are used; however, the results obtained in this work are quite similar to those obtained with ZTO anodes in molecular solvents as the electrolyte, e.g., according to Yuan *et al.*, the previously reported data are 1.40 x 10^{-12} cm^2s^{-1} for neat ZTO and 1.74 x 10^{-10} cm^2s^{-1} for carbon-coated ZTO [42]. Both [Bmpyr][TFSI] and [Mppyr][TFSI] present adequate electrical properties to be used as non-flammable electrolytes in lithium batteries containing ZTO as the anode; hence, their electrochemical properties as well as their lithium storage capacity are as discussed above.

3.2. Electrochemical performance

Typical cyclic voltammograms of the first four cycles for the Zn_2SnO_4 electrode used with [Mppyr][TFSI] and [Bmpyr][TFSI] electrolytes in the batteries tested are depicted in figure 3A and B, respectively.

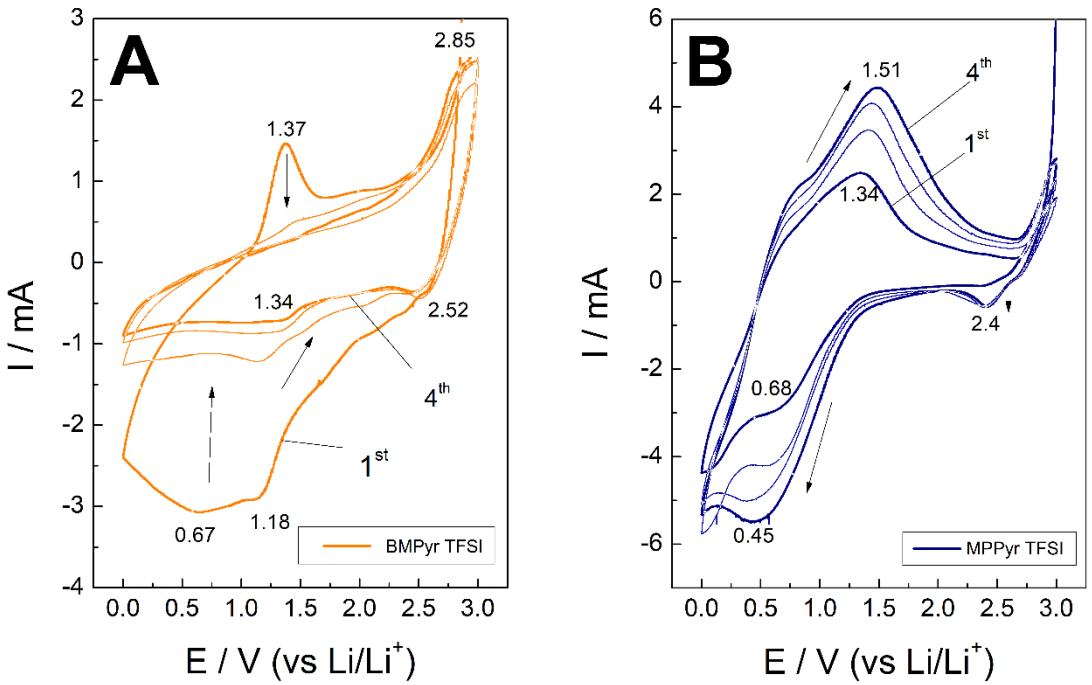

Figure 3. Cyclic voltammograms of the batteries carried out at 0.1 mVs^{-1} using zinc stannate electrodes as working electrode and metallic lithium as reference and counter electrode using **A:** BMPyrTFSI and **B:** MPPyrTFSI as electrolyte.

The cyclic voltammogram of the [Bmpyr][TFSI] sample shows two peaks in the cathodic region at 0.67 V and 1.18 V, and both signals are replaced with a single reduction wave at 1.34 V in the successive cycles. This group of signals can be attributed to an initial multielectronic reduction of

Zn_2SnO_4 to form amorphous Li_2O and Sn, followed by further oxidation of the Sn atoms formed in the working electrode. In the following cycles, the absence of the two signals, the considerably lower charge associated with the reduction process and the potential of the reduction wave indicate that after the initial discharge, only Sn atoms are further reacting, shedding light on the irreversible initial capacity of the battery. The anodic region of the first cycle shows a sharp oxidation peak at 1.37 V, which decreases in intensity with successive cycles. This signal could be evidence of the delithiation process of Li_xSn isolated inside the working electrode framework. In conclusion, the cyclic voltammetry of the [Bmpyr][TFSI] system describes an incomplete and irreversible reduction of Zn_2SnO_4 in the first cycle, forming Sn atoms that are reduced and oxidized in the subsequent cycles.

Figure 3B shows the cyclic voltammogram of the [Mppyr][TFSI] sample. The first cycle shows a reduction signal at 0.68 V, which shifts to a more negative potential in the successive cycles. This signal can be associated with the formation of amorphous Li_2O, generating the respective SEI at the electrode; shifting to an increasingly negative potential can be explained by the further reduction of Sn atoms in the 2nd cycle. The anodic part of the voltammogram shows a wide oxidation signal at 1.34 V, which shifts to a more positive potential and is positioned at 1.51 V in the 4th cycle. This last signal describes the delithiation process taking place in the Li_xSn structures formed during the cathodic process, and the pseudo-reversibility of this signal sheds light on the reversible accumulation of charge in the device.

Chemical equations that describe the overall function of the battery with both studied electrolytes are presented in Eqns. 3 and 4.

$$4Li^+ + Zn_2SnO_4 + 4e^- \rightarrow Sn + 2Li_2O + 2ZnO \quad (3)$$

$$xLi^+ + Sn + xe^- \rightarrow Li_xSn \ (0 \leq x \leq 4.4) \quad (4)$$

Galvanostatic voltage profiles at 0.1 C (0.123 mAg^{-1}) of the Zn_2SnO_4 / Li cell with the ionic liquids as the electrolyte are displayed in figure 4.

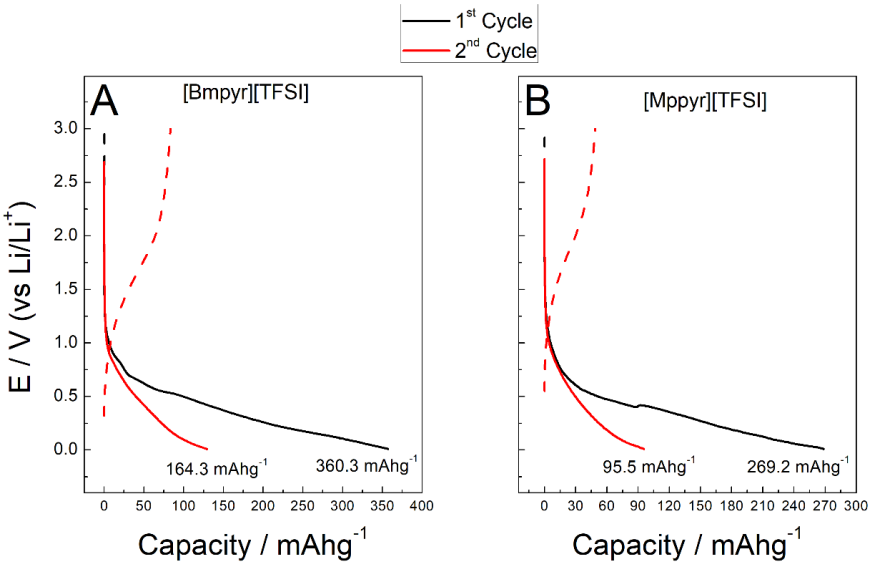

Figure 4. Charge-discharge curves of the batteries at 0,1C using **A**: BMPyrTFSI and **B**: MPPyrTFSI as electrolyte.

As previously mentioned, the study of ZTO as anode using RTIL as electrolyte has not been reported, however, there are a few studies of other anode materials in similar RTIL and can be used as comparison. Zheng and collaborators [43] studied electrochemical intercalation of lithium in graphite, using ammonium based RTIL as electrolyte; the studied cell showed an initial capacity of 67 $mAhg^{-1}$. Later in 2017 Sayah and collaborators [44] studied a Si/Sn-Ni/C/Al composite as anode and [Bmpyr][TFSI] as electrolyte, finding an initial discharge capacity of 219 $mAhg^{-1}$.

Figure 4A shows the galvanostatic charge-discharge curves for the battery assembled with [Bmpyr][TFSI]. The first cycle shows an initial discharge capacity comparable or even superior to many commercial anode alternatives such as graphite (~120 $mAhg^{-1}$ in conventional electrolytes) and lithium titanium oxide (LTO, 170 $mAhg^{-1}$) but a smaller value than other previous results obtained with Zn_2SnO_4 in regular electrolyte preparations. This capacity difference can be explained well by the nature of the electrolyte, whose unique diffusion properties and conduction mechanisms can affect the actual lithium storage. Advantages of the studied systems herein are clearer when comparing to Zheng [43] prototypes and are comparable to recent cells reported by Sayah [44].

The main drawbacks of using ionic liquids as an electrolyte are the sluggish mass transport due to the higher viscosity of the solvent, a fact that has been well explained elsewhere in the literature [37,45]. The second charge process of the battery shows a capacity of 87 $mAhg^{-1}$ and a discharge capacity of 164.3 $mAhg^{-1}$. Considering both discharge capacities shown in the first two cycles, a 55% capacity loss is established.

The charge-discharge battery assembled with [Mppyr][TFSI] (Figure 4B) shows a charge-discharge behaviour similar to that of [Bmpyr][TFSI], revealing a discharge capacity of 269.2 $mAhg^{-1}$ in the first cycle; this value is smaller than that in the last example but still higher than that of common molecular electrolytes. In the second cycle, there is also a decrease in the discharge capacity, reaching 95.5 $mAhg^{-1}$.

It is clear that in both cases a tremendous capacity loss can be observed, and this behaviour is not new, having been evidenced in many previous works [18,19,46–49]. It has been stated that capacity loss is very intimately related to the chemical and morphological properties of Zn_2SnO_4, whose volume changes due to electrochemical reduction dramatically affect the battery performance. The fundamentals of this loss in the studied batteries discussed in the previous section are related to the initial formation of Sn atoms and a highly stable SEI (Li_2O formation) in the first cycle. This electrochemical reduction appears as an irreversible process; hence, the oxidation of Sn to re-form ZTO is thermodynamically impeded in the solvents studied. The storage capacity of the device can be explained by the reduction and oxidation of the formed Sn atoms, whose delithiation process is well defined in the cyclic voltammograms of both [Mppyr][TFSI] and [Bmpyr][TFSI] ionic liquids.

As a tool to understand the chemical processes taking place in the different discharge pathways for each ionic liquid and to understand the subtle differences between [Mppyr][TFSI] and [Bmpyr][TFSI], the number of electrons involved in the discharge process can be roughly estimated by considering the capacities shown in both cycles and using the relation shown in Eqn. 5.

$$n = \frac{C * MM}{F} \qquad (5)$$

where C represents the discharge capacity in $mAhg^{-1}$, MM is the molar mass of the Zn_2SnO_4 (313.47 $gmol^{-1}$), and F is the Faraday constant.

Considering the previous devices, the number of electrons for the [Bmpyr][TFSI] sample in the first cycle is 4.3 electrons for each ZTO molecule and that in the second cycle is 1.9 electrons. These numbers can clarify the reactions and the possible electrochemical storage mechanism taking place in the device.

As discussed previously, the first discharge cycle may start with the reduction of ZTO (Eqn. 3) to form Sn and Li_2O, and according to this model, four electrons are consumed, which is in concordance with the estimation previously presented. The second discharge cycle yields a particular situation in which the reduced Sn atoms are oxidized and then reduced to form an Sn-Li alloy, and according to the estimated number of electrons, can occur via Eqn. 6.

$$2Li^+ + Sn + 2e^- \rightarrow Li_2Sn \qquad (6)$$

On the other hand [Mppyr][TFSI] presents different values for the discharge capacity; hence, the estimated number of electrons involved in the first cycle is 3.3 and that in the following cycles is 1.2. Considering this data and the previous cyclic voltammetry evidence, lithium storage in the [Mppyr][TFSI] device starts with the reduction of ZTO, forming Sn and Li_2O, and then, a reversible redox reaction involving a single electron takes place forming the LiSn alloy, as presented in Eqn. 7.

$$Li^+ + Sn + e^- \rightarrow LiSn \qquad (7)$$

Differences in both electrochemical reactions can be associated with the chemical reactivity of the electrolyte and the ability of each ionic liquid to form a stable SEI and to stabilize certain LiSn alloys that prevail over more reduced forms. In other words, the existence of a butyl chain in $[Bmpyr]^+$ over a propyl chain in $[Mppyr]^+$ determines the stability of the reduced form of ZTO and the rate at which the system is capable of storing lithium ions in the electrode framework; however, the mechanism associated with the stabilization of LiSn alloys and the structure of the SEI formed in these ionic liquids are needed to completely understand the electrochemical process associated with the performance of the device.

4. CONCLUSIONS

In summary, it has been demonstrated that the use of non-flammable and safer electrolytes is possible in lithium batteries based on ZTO, which considering the discharge capacity values obtained can be considered as a potential candidate to replace graphite as the anode in more complex devices. The structure of the cation in the ionic liquid has a direct impact on the electrochemical performance of the device, changing the pathway in which the device stores lithium ions. While both ionic liquids allow a first discharge driven by the multielectronic reduction of ZTO, [Bmpyr][TFSI] presents a two-electron reduction/oxidation in the second cycle, and [Mppyr][TFSI] exhibits only a monoelectronic redox reaction to form LiS_n. The electrochemical impedance spectroscopy measurements shed light on the true relevance of using pyrrolidinium ionic liquids over common imidazolium-based salts. The characterization in terms of the diffusion coefficient and charge transfer resistance allow us to conclude that mass transport in [Bmpyr][TFSI] is more suitable among the alternatives studied herein.

ACKNOWLEDGEMENTS
The authors give thanks to the organizations that funded the present work, specifically FONDECYT 3170333 (DQ) and FONDECYT 3180061 (JH)

References

1. P. G. Bruce, B. Scrosati, J.-M. Tarascon, *Angew. Chem. Int. Ed*., 47 (2008) 2930.
2. B. Scrosati, J. Garche, *J. Power Sources,* 195 (2010) 2419.
3. Vincent Dusastre, *Materials for Sustainable Energy*, Macmillan Publishers Ltd, (2010) London, UK.
4. J.B. Goodenough, K.-S. Park, *J. Am. Chem. Soc.,* 135 (2013) 1167.
5. C. -X. Zu, H. Li, *Energy Environ. Sci*., 4 (2011) 2614.
6. Z. Gao, H. Sun, L. Fu, F. Ye, Y. Zhang, W. Luo, Y. Huang, *Adv. Mater.,* 30 (2018) 1705702.
7. Y. Sun, N. Liu, Y. Cui, *Nat. Energy,* 1 (2016) 16071.
8. N. Nitta, F. Wu, J. T. Lee, G. Yushin, *Mater. Today,* 18 (2015) 252.
9. F. Wu, G. Yushin, *Energy Environ. Sci.,* 10 (2017) 435.
10. D. Bresser, S. Passerini, B. Scrosati, *Chem. Commun*., 49 (2013) 10545.
11. S. Goriparti, E. Miele, F. De Angelis, E. Di Fabrizio, R. Proietti Zaccaria, C. Capiglia, *J. Power Sources,* 257 (2014) 421.
12. Y. Nishi, *Chem. Rec*., 1 (2001) 406.
13. P. Rozier, J.M. Tarascon, *J. Electrochem. Soc*., 162 (2015) A2490.
14. J. -H. Lim, H. Bang, K. -S. Lee, K. Amine, Y. -K. Sun, *J. Power Sources,* 189 (2009) 571.
15. J. Wang, X. He, E. Paillard, N. Laszczynski, J. Li, S. Passerini, *Adv. Energy Mater*., 6 (2016) 1600906.
16. A. Birrozzi, N. Laszczynski, M. Hekmatfar, J. von Zamory, G. A. Giffin, S. Passerini, *J. Power Sources,* 325 (2016) 525.
17. T. Hashemi, F. Golestani-Fard, J. Avanessian, *J. Electrochem. Soc*., 134 (1987) 1591.
18. X. J. Zhu, L. M. Geng, F. Q. Zhang, Y. X. Liu, L. B. Cheng, J. *Power Sources,* 189 (2009) 828.
19. A. Rong, X. P. Gao, G. R. Li, T. Y. Yan, H. Y. Zhu, J. Q. Qu, D. Y. Song, *J. Phys. Chem., B* 110 (2006) 14754.
20. L. P. Wang, Y. Zhao, C. Wei, C. Wong, M. Srinivasan, Z. J. Xu, *J. Mater. Chem*. *A*, 3 (2015) 14033.
21. J. Jaguemont, L. Boulon, Y. Dubé, *Appl. Energy,* 164 (2016) 99.
22. K. Takada, Acta Mater., 61 (2013) 759.
23. A. Lewandowski, A. Świderska-Mocek, *J. Power Sources,* 194 (2009) 601.
24. L. Le, T. Vo, K. Ngo, S. Okada, F. Alloin, A. Garg, P. Le, *J. Ind. Eng. Chem*., 10 (2004) 1086.
25. M. Armand, F. Endres, D. MacFarlane, H. Ohno, B. Scrosati, *Nat. Mater*., 8 (2009) 621.
26. L. Lu, X. Han, J. Li, J. Hua, M. Ouyang, *J. Power Sources,* 226 (2013) 272.
27. J. Kalhoff, G.G. Eshetu, D. Bresser, S. Passerini, *ChemSusChem,* 8 (2015) 2154.
28. R. A. Sheldon, *Green Chem*., 7 (2005) 267.
29. D. Ruiz-León, R. E. Avila, C. J. Venegas, *J. Chil. Chem. Soc*., 60 (2015) 3029.
30. J. Kalhoff, G. G. Eshetu, D. Bresser, S. Passerini, *ChemSusChem,* 8 (2015) 2154.
31. J. L. Anthony, J. L. Anderson, E. J. Maginn, J. F. Brennecke, *J. Phys. Chem*. *B,* 109 (2005) 6366.
32. A. Lewandowski, M. Galiński, *J. Phys. Chem. Solids,* 65 (2004) 281.
33. S. Theivaprakasam, D. MacFarlane, S. Mitra, *Electrochim. Acta,* 180 (2015) 737.
34. J. Zheng, M. Gu, H. Chen, P. Meduri, M. H. Engelhard, J. -G. Zhang, J. Liu, J. Xiao, *J. Mater. Chem. A,* 1 (2013) 8464.
35. S. J. An, J. Li, C. Daniel, D. Mohanty, S. Nagpure, D.L. Wood, *Carbon,* 105 (2016) 52.
36. H. -B. Han, S. -S. Zhou, D. -J. Zhang, S. -W. Feng, L. -F. Li, K. Liu, W. -F. Feng, J. Nie, H. Li, X.-J. Huang, *J. Power Sources,* 196 (2011) 3623.
37. A. Swiderska-Mocek, *Electrochim. Acta,* 132 (2014) 504.

38. L. Le, T. Vo, K. Ngo, S. Okada, F. Alloin, A. Garg, P. Le, *J. Mol. Liq*., 271 (2018) 769.
39. H. Srour, H. Rouault, C.C. Santini, *J. Electrochem. Soc*., 160 (2013) A781.
40. H. Srour, L. Chancelier, E. Bolimowska, T. Gutel, S. Mailley, H. Rouault, C. C. Santini, *J. Appl. Electrochem*., 46 (2016) 149.
41. W. S. Yuan, Y. W. Tian, G. Q. Liu, *J. Alloys Compd*., 506 (2010) 683.
42. M. Holzapfel, C. Jost, P. Novák, *Chem. Commun*., (2004) 2098.
43. H. Zheng, K. Jiang, T. Abe, Z. Ogumi, *Carbon,* 44 (2006) 203.
44. S. Sayah, F. Ghamouss, F. Tran-Van, J. Santos-Peña, D. Lemordant, *Electrochim. Acta,* 243 (2017) 197.
45. C. Yan, J. Yang, Q. Xie, Z. Lu, B. Liu, C. Xie, S. Wu, Y. Zhang, Y. Guan, *Mater. Lett*., 138 (2015) 120.
46. X. Hou, Q. Cheng, Y. Bai, W.F. Zhang, *Solid State Ionics,* 181 (2010) 631–634.
47. W. Song, J. Xie, W. Hu, S. Liu, G. Cao, T. Zhu, X. Zhao, *J. Power Sources,* 229 (2013) 6–11.
48. B. -Y. Wang, H. -Y. Wang, Y. -L. Ma, X. -H. Zhao, W. Qi, Q. -C. Jiang, *J. Power Sources,* 281 (2015) 341.

© 2021 The Authors. Published by ESG (www.electrochemsci.org). This article is an open access article distributed under the terms and conditions of the Creative Commons Attribution license (http://creativecommons.org/licenses/by/4.0/).